

11th CIRP Conference on Photonic Technologies [LANE 2020] on September 7-10, 2020

Preliminary machine learning analysis and high-speed thermographic visualization of the laser polishing process

Jack Beyfuss^{a,b,†}, Evgueni Bordatchev^{b,a,†,*}, O. Remus Tutunea-Fatan^{a,b,*}

^a Department of Mechanical and Materials Engineering, Western University, London, ON, N6A 5B9 Canada

^b National Research Council of Canada, 800 Collip Circle, London, ON, N6G 4X8 Canada

* Corresponding author. Tel.: +1-226-688-5604; fax: +1-519-430-7064. E-mail address: evgueni.bordatchev@nrc-cnrc.gc.ca, rtutunea@eng.uwo.ca

Abstract

Laser polishing (LP) is an advanced manufacturing process for improving surface quality via laser remelting of the surface topography of the material. In this preliminary study, a high-speed thermographic imager was coaxially installed on a LP system and was used to capture the thermodynamics of the laser-material interactions under various process conditions. A visualization algorithm was developed and used to monitor the LP process dynamics along the laser path trajectory. This approach enables the analysis of LP process stability by means of reliable informational features of the individual images. Further, unsupervised machine learning analysis (Bayesian classifier) was used to reduce the number of informational variables/statistical characteristics of the images without compromising process predictability. These two techniques were applied for both monitoring and classification of the LP line experiments performed with a laser power of {5, 20, 35} W and a scanning speed of 75 mm/s. The preliminary results demonstrate the high potential of machine learning analysis towards the optimization and control of the LP process.

© 2020 The Authors. Published by Elsevier B.V.

This is an open access article under the CC BY-NC-ND license (<http://creativecommons.org/licenses/by-nc-nd/4.0/>)

Peer-review under responsibility of the Bayerisches Laserzentrum GmbH

Keywords: laser polishing; thermographic imaging; on-line monitoring; machine learning; Bayesian classifier

1. Introduction

Laser polishing (LP) is an emerging manufacturing process that entails the use of laser radiation to melt the surface of functional parts such as tooling inserts [1-4]. During LP, workpiece material melts into a pool and solidifies rapidly into a smooth surface due to complex and overlapping thermodynamic phenomena induced by a constantly travelling laser beam. The quality of the post-LP surface critically depends on several process parameters, such as: laser power, travelling speed, focal distance, and track step over. The synergetic effect of these process parameters contributes to a thermodynamic equilibrium between solid, molten and resolidified material. Along these lines, several research studies have already emphasized the importance of the on-line monitoring of the actual temperature in the laser-material interaction zone. This information is needed for the identification of current process conditions and for further

control and optimization of the LP performance with respect to (wrt) desired and/or best achievable surface quality. Pyrometers have been commonly used for LP process monitoring and control [5, 6]. In this application, process temperature is continuously measured (possibly with a sampling frequency of 600 Hz) in the middle of the focal line and proportional-integral-derivative close-loop control is applied in real-time to laser power in order to maintain a constant surface temperature. Prior studies have shown that LP process temperature can be controlled within $\pm 15 \dots 20$ K.

Industry 4.0-based next generation manufacturing integrates cyber-physical systems, artificial intelligence, big data analysis, and modern manufacturing technologies with advanced laser processing [7]. Among the numerous technological examples developed and implemented so far, high-speed midwave-infrared (MWIR) camera has been used to monitor and evaluate the laser welding process [8]. For this purpose, a MWIR camera was mounted coaxially with laser

welding optics and it was used to record thermographic images of the process with a sampling frequency of 500 Hz and within a field of view of 9x9 mm². From there, principal component analysis under a concept of unsupervised machine learning and image geometry-based parameters were used to extract the image features characterized by a high informational/data analysis value. In this context, it was found that the analyzed geometrical features were highly sensitive to the changes of the experimental conditions and thereby allowed detection and separation of the investigated welding defects with 99.9% accuracy. This welding-focused approach seems suitable to the LP process, especially since the thermodynamic performance of laser-material interactions as well as their thermographic imaging exhibit significant similarities.

The present feasibility study is focused on the thermographic imaging, visualization, analysis, and machine learning-based classification (*e.g.*, Bayesian) of the LP process. Several LP experiments were performed under various process parameters while thermographic images of the laser-material interaction zone were recorded at a high-speed (> 3 kHz). The captured images were then restructured into a spatial 2D process visualization. Furthermore, several image geometry-based features were extracted to evaluate the LP process performance wrt the laser power. Building upon the acquired knowledge, a Bayesian classifier [9] was used to demonstrate the ability to perform unsupervised LP process monitoring, optimization, and control.

2. LP experimental set-up

Fig. 1 shows a picture of the LP experimental setup consisting of laser, laser beam delivery optics, laser scanner, and 3-axis motion system. The continuous wave fiber laser (YLR-100-SM-CS, from IPG Photonics Inc., USA), having a maximum power of 100 W, was operated with a wavelength of 1070 nm. Laser beam was collimated and delivered to a 2D galvanometric laser scanner (exelliSCAN 14, from SCANLAB GmbH, Germany) equipped with a 254 mm scan f-theta lens. A camera adapter was placed between the collimator and laser scanner where interchangeable optical and thermographic cameras were mounted. The optical camera was used for visual alignment and precise setting of the laser beam and workpiece. Thermographic imaging was performed using a MWIR camera (TACHYON 16K, New Infrared Technologies, S.L., Spain) capable of acquiring 128x128 pixels images with a maximum of 2000 fps within a wavelength ranging between 1 and 5 μ m.

The 55x55x5 mm³ workpiece made of H13 tooling steel was mechanically mounted on a System 3R (from Mikron AGIE Charmilles AG, Switzerland) rapid-clamping feature attached to a Y-axis linear stage. This clamping arrangement enables an advanced ability to position/reposition the workpiece with high repeatability ($\pm 1 \mu$ m) required for pre- and post-LP surface topography acquisition. In addition, the pre-ground workpiece top surface was aligned along the X- and Y-axes within a $\pm 2 \mu$ m deviation by means of a touch probe caliper. To create an oxygen-free processing zone, a constant flow of Ar was directed to the laser-material interaction zone. The 3-axis motion system was made of two linear drives operating along X- and Y-axes and a ball-screw driven Z-axis.

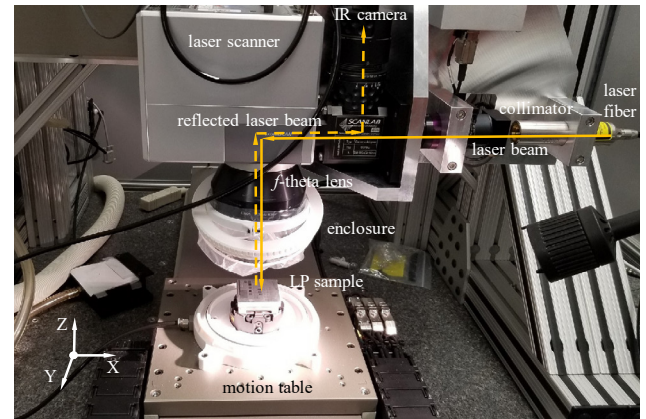


Fig. 1. Experimental set-up.

The laser scanner and optics were mounted on X- and Z-axes and attached to the granite bridge. The workpiece was located on Y-axis and was affixed to a granite table for enhanced thermal stability. All electronic components (motion controllers, laser scanner and laser control unit) were connected to the main motion control unit (Aerotech, Inc., USA).

3. Thermographic image analysis methodology

The thermographic image analysis was divided in three processing steps. At first, LP experiments were performed in such a way that three sets of three 5 mm long lines were polished with scanning speeds of {25, 50, 75} mm/s and laser powers of {5, 20, 35} W, however only experiments with a scanning speed of 75 mm/s were analyzed in this preliminary study. The LP process was recorded with the Tachyon MWIR camera/software for each set of LP lines. Image acquisition was performed with a sampling rate of over 3000 fps and a frame size of 64x64 pixels. The acquired data was saved into a file with a particular structure of common parameters (*i.e.*, temperature range) and comprised of image frames and corresponded time stamps.

The second phase of thermographic image analysis was allotted to the determination of the informational features to be used for further process analysis and classification. In the context of the present feasibility study, only areal image projection (*e.g.*, representing an area of the laser-material interactions including melt pool and heat affected zone) was used. By contrast, spatial and amplitude parameters of the thermographic images were intentionally left out for future analysis. In a more general sense, this step represents nothing but a dimension reduction from a 64x64 data matrix associated with each image to a vector characterized by few informational features. This transformation is important for the augmentation of the computational efficiency as well as for the subsequent on-line monitoring, optimization, and control of the LP process.

Fig. 2 depicts definitions of the temperature contour-based informational features for each image frame. Mathematically, the temperature contour was defined as a 64x64 binary matrix for each of the N thermographic images (after the application of a certain temperature threshold T_{tr}) as

$$h_k(i, j) = \begin{cases} 1, & \text{when } T_k(i, j) \geq T_{tr} \\ 0, & \text{when } T_k(i, j) < T_{tr} \end{cases}, \quad i, j = 1 \dots 64, k = 1 \dots N \quad (1)$$

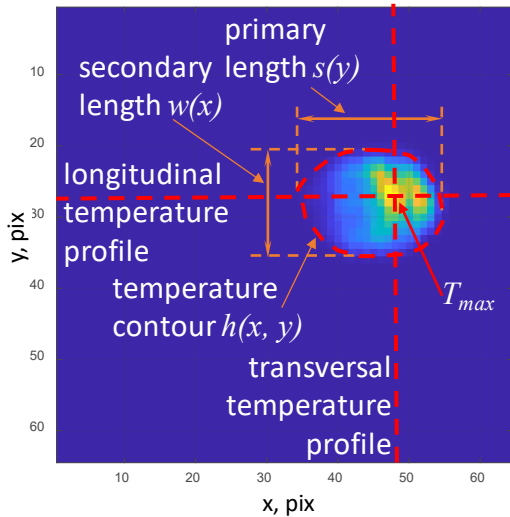


Fig. 2. Definition of the temperature contour-based informational features.

It was evident that each temperature contour $h(i, j)$ has an elliptical shape and therefore three most obvious informational features can be used, such as

- area of laser-material interaction zone:

$$A_k = \sum_{i,j} h_k(i, j), \quad i, j = 1 \dots 64, \quad k = 1 \dots N, \quad (2)$$

- length of the laser-material interaction zone calculated from longitudinal temperature profile:

$$s_k = \sum_i h_k(i, j), \quad i = 1 \dots 64, \quad j \text{ of } T_{k,max}, \quad k = 1 \dots N, \quad (3)$$

- width of the laser-material interaction zone calculated from transversal temperature profile:

$$w_k = \sum_j h_k(i, j), \quad j = 1 \dots 64, \quad i \text{ of } T_{k,max}, \quad k = 1 \dots N. \quad (4)$$

During the third phase, a MATLAB-based function was developed to extract all informational features defined in Eqs. 2-4 for each LP experiment. To achieve this, these features were rearranged from a frame-driven index ($k = 1 \dots N$) into a discrete function related to the travel distance of 5 mm for each LP line. This was accomplished by using a timestamp and a constant scanning speed, a method that enabled the ability to synchronize experimental data in space (*i.e.*, along the LP line) instead of the time domain. Moreover, the data associated with the first and last 0.5 mm of each LP line was removed in an attempt to eliminate any transient behavior as well as to ensure reliable analysis of the steady LP process only. The resulting $A(x)$, $s(x)$, $w(x)$ data were further used for the LP process visualization, analysis, and Bayesian classification.

4. Visualization of LP process performance

In order to visualize the LP process, the transversal temperature profile $h_k(i, \bullet)$ extracted from each k -frame at T_{max} (and all profiles) was generated as a function of the travel distance. Fig. 3 illustrates an image-based LP process visualization characterized by {5, 20, 35} W laser power and 75 mm/s travel speed. At 5 W laser power, the contour of the molten pool/heat affected zone appeared jagged with a highly non-uniform boundary. This is most likely a consequence of the shallow surface melting phenomenon that is inevitably present at low laser power levels.

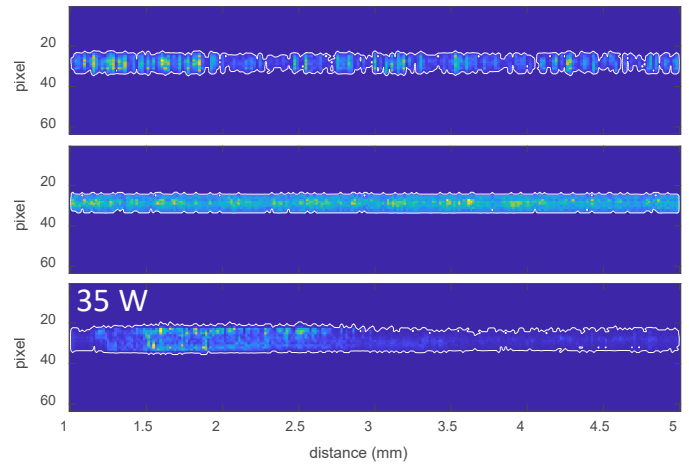


Fig. 3. LP process visualization with {5, 20, 35} W laser power and 75 mm/s.

By contrast, LP process appears to be more stable at 20 W (more uniform and consistent boundaries of the temperature envelope). Finally, significant variations in the thermodynamic equilibrium of the LP process are present at 35 W and they appear to significantly influence the formation of instabilities in the polished surface topography. Two additional observations can be made in this high power case: i) the temperature envelope is characterized by low frequency variations of its boundaries, and ii) occasional flares in the temperature and contour area are present. This latter aspect may represent an indicator of the LP quality and performance related to the initial surface topography, process parameters, physical-mechanical properties of the workpiece material as well as polished surface topography.

5. Analysis of LP using defined informational features

Fig. 4 shows the functional variation of the informational features defined in Section 3 (*i.e.*, $A(x)$, $s(x)$, and $w(x)$) that are characteristic to the laser-material interaction zone associated with the three LP lines made with {5, 20, 35} W laser power and 75 mm/s travel speed. Clearly, the geometric properties introduced in Section 3 are strongly correlated with the applied laser power. All three analyzed informational features exhibit a similar behavior wrt laser power: a) the actual values become higher when laser power increases, b) value-power functional is nonlinear: the increase from 20 W to 35 W is significantly larger than that from 5 W to 20 W, c) visually/qualitatively, their spatial signature along LP line length correlates with process visualization (Fig. 3), and d) these features are interdependent as their signatures appear to be very similar.

6. Bayesian classification of the applied laser power

In order to determine the applicability of the three analyzed informational features ($A(x)$, $s(x)$, $w(x)$) for machine learning-based monitoring, optimization and control of the LP process, a classic pattern recognition analysis (aka Bayesian classifier) [9] was applied. In broad strokes, pattern recognition analysis is based on the linear discriminant theory and enables the selection of the best combination of informational features within the n -dimensional informational space. This is meant to

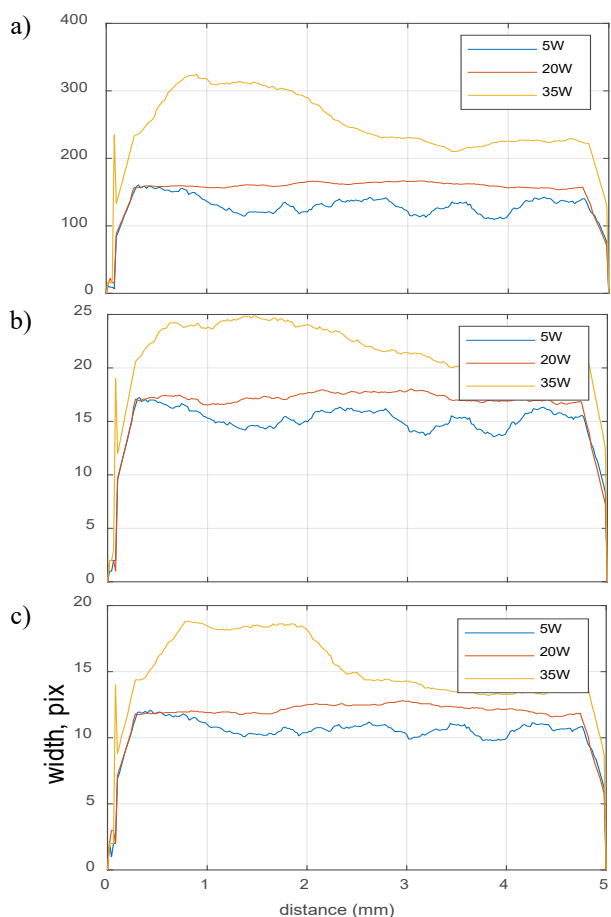


Fig. 4. Functional dependence of informational features wrt the laser power.

provide mathematical rules as linear decision functions to be embedded into control hardware for real-time monitoring, diagnostics and control of the LP process. Three Bayesian classifiers were computed for the informational spaces $\{A(x), s(x)\}$, $\{A(x), w(x)\}$, and $\{s(x), w(x)\}$, with a quality of classification of 79.3%, 84.9%, and 78.2%, respectively. The classification results are presented in Fig. 5.

7. Summary and conclusions

This study demonstrates both the feasibility and applicability of high-speed thermographic imaging for visualization, analysis, and machine learning-based Bayesian classification of the LP process. In this context, several conclusions became apparent:

- The three proposed informational features reliably correlate with laser power variations and they can be used in the Bayesian classification for on-line monitoring, optimization, and control of the LP process.
- Pattern recognition analysis grants the ability to choose the most adequate informational features
- This study sets the informational foundation towards the future integration of the LP process into the Industry 4.0 framework

Acknowledgements

This study is the result of collaboration between the National

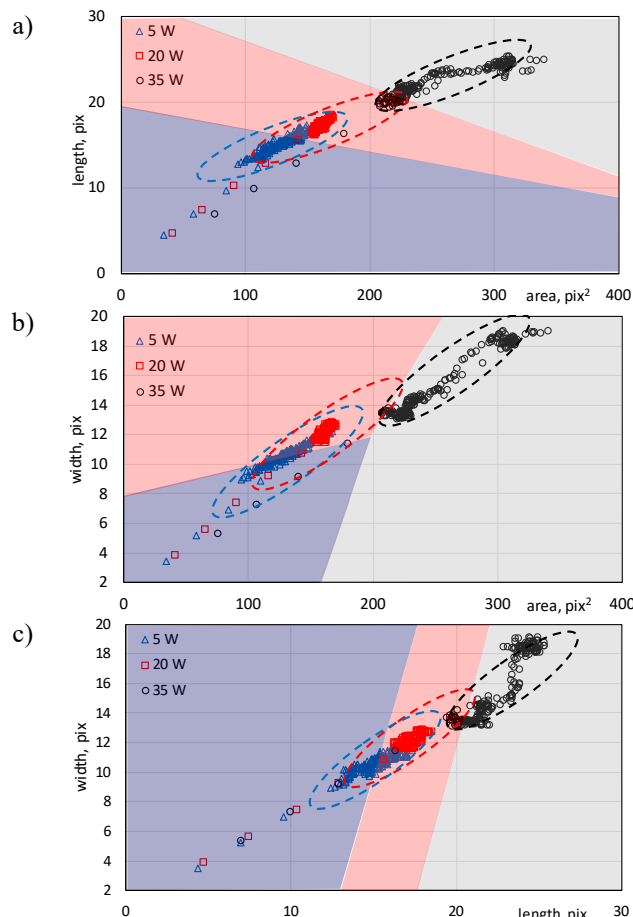


Fig. 5. Bayesian classifiers for $\{A(x), s(x)\}$, $\{A(x), w(x)\}$, and $\{s(x), w(x)\}$.

Research Council of Canada (London, Ontario) and Western University (London, Ontario). Partial financial support was also provided by the Natural Sciences and Engineering Research Council (NSERC) of Canada.

† these authors contributed equally to this study

References

- [1] Willenborg E. Polishing with laser radiation. In: Poprawe R, editor: Tailored Light 2: Laser Application Technology; 2011. p. 196-202.
- [2] Temmler A, Willenborg E, Wissenbach K. Laser polishing. Proceedings of SPIE 2012; vol. 8243, paper 82430W, 13 p.
- [3] Pfefferkorn FE, Duffie NA, Li X, Vadali M, Ma C. Improving surface finish in pulsed laser micro polishing using thermocapillary flow. CIRP Annals – Manuf Tech 2013;62:203-6.
- [4] Bordatchev EV, Hafiz AMK, Tutunea-Fatan OR. Performance of laser polishing in finishing of metallic surfaces. International Journal of Advanced Manufacturing Technologies 2014;73:35–52.
- [5] Heidrich S, Richmann A, Schmitz P, Willenborg E, Wissenbach K, Loosen P, Poprawe R. Optics manufacturing by laser radiation, Optics and Lasers in Engineering 2014;59:34-40
- [6] Weigarten C, Schmickler A, Willenborg E, Wissenbach K. Laser polishing and laser shape correction of optical glass, Journal of laser applications 2017;29(1): paper 011702, 9 p.
- [7] Lotzman T, Wenzel F, Karsunke U, Kozak, K. For Industry 4-0, visualization and machine learning can be combined to enhance laser processing. Laser Focus World 2017;January:87-9.
- [8] Knaak C, Thombansen U, Abels P, Kröger M. Machine learning as a comparative tool to determine the relevance of signal features in laser welding. Procedia CIRP 2018;74:623-7
- [9] Tou JT, Gonzalez RC. Pattern recognition principles. Addison-Wesley, Reading, MA, 1974.